AIP Advances

Synthesis, characterization and magnetic properties of ultrafine Co3O4 octahedra

Y. H. Chen, J. F. Zhou, D. Mullarkey, R. O'Connell, W. Schmitt, M. Venkatesan, M. Coey, and H. Z. Zhang

Citation: AIP Advances **5**, 087122 (2015); doi: 10.1063/1.4928494
View online: http://dx.doi.org/10.1063/1.4928494
View Table of Contents: http://scitation.aip.org/content/aip/journal/adva/5/8?ver=pdfcov
Published by the AIP Publishing

Synthesis, characterization and magnetic properties of ultrafine Co_3O_4 octahedra

Y. H. Chen,[1] J. F. Zhou,[1] D. Mullarkey,[1] R. O'Connell,[1] W. Schmitt,[2] M. Venkatesan,[1] M. Coey,[1] and H. Z. Zhang[1,a]
[1]*School of Physics and Centre for Research on Adaptive Nanostructures and Nanodevices (CRANN), Trinity College, Dublin 2, Ireland*
[2]*School of Chemistry, Trinity College, Dublin 2, Ireland*

(Received 20 March 2015; accepted 17 July 2015; published online 7 August 2015)

Octahedral Co_3O_4 nanoparticles were synthesised in an aqueous ammonia solution using hexagonal β-$Co(OH)_2$ nanoplates as starting materials. Electron microscopy analysis indicates that the Co_3O_4 particles have diameters of 20-40 nm and adopt a well-crystallized cubic spinel structure. The octahedral habit was verified by high angle annular dark field imaging. High resolution electron microscopy results revealed that the long axis of the octahedral Co_3O_4 nanoparticles coincides with crystallographic <111> direction and the facets are the {111} planes. Magnetization measurements reveal antiferromagnetic ordering below 10 K, with a paramagnetic Curie temperature of 3 K and a paramagnetic susceptibility that is double that expected for high-spin Co^{2+}. The results show that a substantial fraction of the B-site Co^{3+} in the nanoparticles is in a high-spin state. [http://dx.doi.org/10.1063/1.4928494]

I. INTRODUCTION

The mixed-valence oxide Co_3O_4 is a p-type semiconductor with the normal spinel structure that has been used in lithium-ion batteries,[1,2] gas sensors[3] and catalysts.[4] The magnetic structure was described 50 years ago by Roth.[5] High-spin Co^{2+} occupies the tetrahedral A-sites of the spinel structure, while low-spin Co^{3+} occupies the octahedral B-sites. The Co^{3+} is nonmagnetic, with a $3d^6$ S = 0 configuration, whereas only the Co^{2+} $3d^7$ with S = 3/2 has a magnetic moment. The A – A exchange interactions are weak and antiferromagnetic. They are unfrustrated in the spinel structure, and the oxide orders antiferromagnetically with a Néel temperature of 40 K, which is comparable to the magnitude of the paramagnetic Curie temperature (53 K). The magnetic properties of nanosized Co_3O_4 materials depend on the shape, size and crystallization conditions of the nanoparticles,[6–12] and are particularly sensitive to the spin state of the Co^{3+} ions near the surface.[13] A variety of novel Co_3O_4 nanostructures with variable morphologies including hollow nanospheres,[14] nanowires,[15] nanoparticles,[7] and nanotubes[6,9] have been prepared, and anomalous magnetic properties has been reported, due to their surface condition.

Octahedral single-crystal Co_3O_4 has a {111} habit exposing more close-packed planes and exhibiting more stable electrochemical performances than other shapes of Co_3O_4.[16] The synthesis of single crystalline octahedral Co_3O_4 nanostructures usually involves the chemical reaction of Co^{2+} ions and an alkali base followed by subsequent thermal treatment.[1] Single crystalline Co_3O_4 materials can also be synthesized by one-pot hydrothermal methods.[16] Previous syntheses sometimes resulted in a large size distribution of particle diameters from few nanometres to few micrometres.[17,18] As a consequence, magnetic properties of Co_3O_4 nanostructures were often measured on mixtures of particles with large size variations and thus the investigation of size-dependent

[a]Electronic mail: hongzhou.zhang@tcd.ie

phenomena was hampered. Therefore, a mild and simple synthetic procedure which results in uniform, homogeneous and well-crystallized Co_3O_4 nanoparticles are desirable.

In this paper, a simple hydrothermal synthetic procedure is used to prepare crystalline nanoscale Co_3O_4 particles with octahedral morphology that form at comparatively low temperatures. The particles are characterized by electron microscopy, and magnetic properties are investigated.

II. EXPERIMENTAL PROCEDURE

The applied synthetic procedure, involved two hydrothermal steps to prepare the $Co(OH)_2$ nanoplate-like starting material and the final Co_3O_4, nanoparticles, respectively. At the first stage, 0.2 mol $CoCl_2{\cdot}6H_2O$ was dissolved in 20 mL deionized water and while stirring, 20 mL of a 0.5 M NaOH solution was added to the reaction mixture. This solution was then stirred for further five minutes followed by heating at a temperature of 120 ^oC for 6 hours in a sealed teflon-lined autoclave. The autoclave was allowed to cool to room temperature. A brown gel-like precipitate was collected from the bottom of the autoclave and was washed with distilled water and ethanol. This precipitate was then dried in an oven at 80 ^oC for 24 hours after which a dark brown, homogeneous powder was obtained. This was used as the starting material for the preparation of Co_3O_4 nanoparticles. In the second stage of the process, 0.02 g of this powder was dispersed 40 mL of an aqueous ammonia solution (2.5 wt%). The reaction mixture was then sealed in a 50 mL teflon-sealed steel autoclave and heated to 120 ^oC for 6 h. After the reaction, a black powder was obtained. It was filtered off and washed several times with deionised water and used for characterization.

A BRUKER D8 ADVANCE X-ray diffractometer using graphite monochromatized Cu K_α radiation was used to perform X-ray powder diffraction (XRD) measurements. A scanning rate of $0.02^o\,s^{-1}$ was applied and the patterns were recorded in the 2θ range of 10-80^o. A Carl Zeiss Ultra scanning electron microscope (SEM) was used to image the morphologies of the cobalt oxide nanoparticles. The SEM allowed us to perform energy dispersive X-ray spectroscopy (EDX) of the sample. Before imaging the samples by SEM and transmission electron microscope (TEM), the samples were drop cast from solution using a pipette onto an amorphous carbon film and allowed to dry in air. The TEM used for these experiments was a 300 kV FEI Titan capable of performing both electron energy loss spectroscopy (EELS) and EDX . In all cases a wide selection of individual nanoparticles was examined to determine representative structures and morphologies. Magnetization measurements were made using a 5-Tesla Quantum Design MPMS 5T SQUID magnetometer.

III. RESULTS AND DISCUSSION

Figure 1 shows the typical XRD patterns of the starting material and the final product. The recorded diffraction peaks of the starting material contain two phases. The trigonal β-$Co(OH)_2$ phase (JCPDS file No. 30-0443) was the predominant phase, plus a small amount of rhombohedral CoOOH phase (JCPDS 73-1213), as shown in Fig. 1(a). All the diffraction peaks of the final products can be exclusively indexed to the cubic spinel Co_3O_4 structure (JCPDS file No. 42-1467, space group: Fd-3m (227); lattice constant: a = 0.808 nm).The lattice constant calculated from the XRD pattern is 0.81 nm, which is coincident with the data. The grain size of the final product, which is 28-30 nm, has been estimated from the Scherrer formula.[19]

As reported in $FeNi(OH)_2$ plates[20] and other related works on $Co(OH)_2$ plates,[21] the starting material, i.e. $Co(OH)_2$, has a hexagonal-like thin plate shape with close-packed {001} crystallographic planes as its surface and bottom surfaces. Figure 2(a) is a typical TEM image of such a plate with its hexagonal axis parallel to the beam direction. An enlarged edge profile of the discs is shown in Fig. 2(b), which reveals the close-packed {001} planes. The corresponding electron diffraction patterns corroborate the hcp β-$Co(OH)_2$ structure viewed along the <001> direction. The side-view of the plates in Fig. 2(d) shows chamfered edges. As discerned from the lattice arrangement in the high-resolution TEM (HRTEM) image in Fig. 2(e), the side facets can be indexed as one of the {110}, {010} or {100} planes (equivalent planes in the hcp structure, perpendicular to the hexagonal {001} plane). For the chamfered edge, the other two facets adjacent to the {110} side facet are

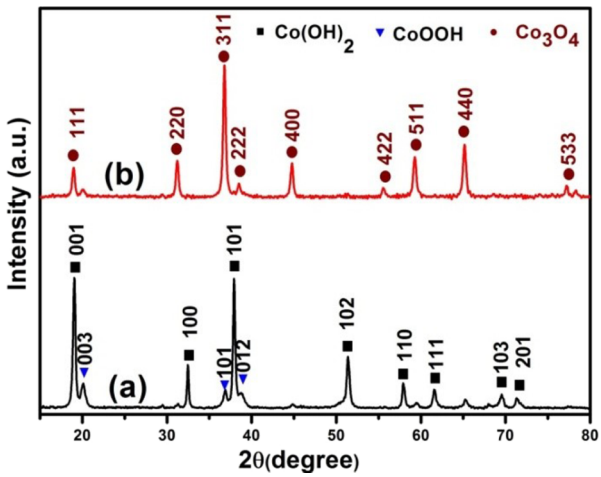

FIG. 1. XRD pattern of (a) starting β-$Co(OH)_2$ and (b) final Co_3O_4 products obtained after reaction for 6 h at 120 °C.

belonged to the {113} group, which is deduced from the interplanar distancesand the proper angles subtended by them. The angle between the edges are 134°, corresponding to the angles subtended by the normal of {110} and {113} planes. A model of the plate is shown in Fig. 2(f). The plate normal is along the <001> direction with the {001} plane as its hexagonal top and bottom facets (in light blue). The side facets are the {110} facet (in pink) and the {113} facet (in dark blue).

Figure 3(a) shows a typical SEM image of the product that formed after a reaction of 6 hours at 120 °C in dilute ammonia. The product is mostly composed of octahedra with edge lengths ranging from 20to 50 nm. The size distribution of the octahedra is depicted in Fig. 3(b), which showsa Gaussian profile with an average size of 30 nm. The mean dimension of the octahedra measured from the SEM images is consistent with the value calculated from the XRD pattern using the Scherrer formula. These XRD and SEM analyses indicate that the octahedra are single crystals without internal grain structures. This is further confirmed by TEM characterisation as described below. A typical bright-field TEM image is shown in Fig. 3(c), further confirming that the particles exhibit a uniform size with evident octahedral shape. The electron diffraction pattern (EDP) taken from the

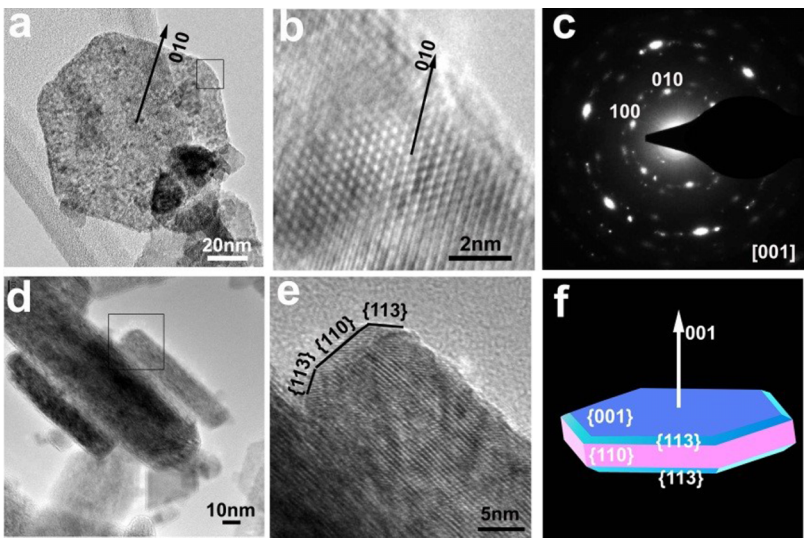

FIG. 2. (a) TEM of a plane-view of plate hexagonal $Co(OH)_2$ and its (b) Enlarged HRTEM image on edge and (c) its EDP. (d) TEM of an edge-view of plate hexagonal and its (e) Enlarged HRTEM image on edge and (f) Schematic drawing of a plate and its indexed facets.

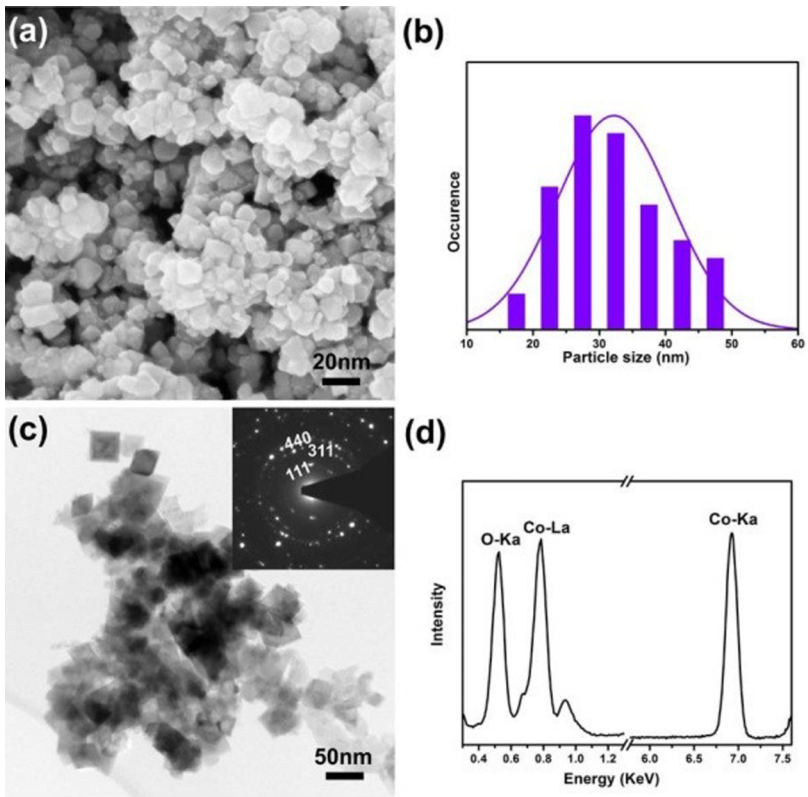

FIG. 3. Products after reaction in dilute ammonia solution (2.25 wt %) at 120 ^{o}C for 6 h. (a) Typical SEM image, (b) Diameter distribution, (c) Typical TEM image and its corresponding EDP and (d) EDX spectrum.

ensemble of the nanocrystals (the inset in Fig. 3(c)) corresponds to a polycrystalline pattern that arises from the aggregation of these nanosized cubic spinel structure. The diffraction rings, from the inner to the outer sphere, are attributed to the {111}, {311} and {440} planes of cubic Co_3O_4 respectively. The EDX spectrum taken from the same area is provided in Fig. 3(d), indicating that the nanoparticles contains Co and O with a Co/O ratio of about 3/4.

The lattice-resolved image is shown in Fig 4(a) which was taken from the area of an octahedron indicated in the inset. The lattice spacing is 0.30 nm and corresponds to interplanar spacing along the <110> direction. It suggests that the edge of the octahedral base (the square) is along <110> direction and the zone axis is perpendicular to the base that is along <111> direction.It is interesting to note that all the octahedral particles examined in the HRTEM experiments (about

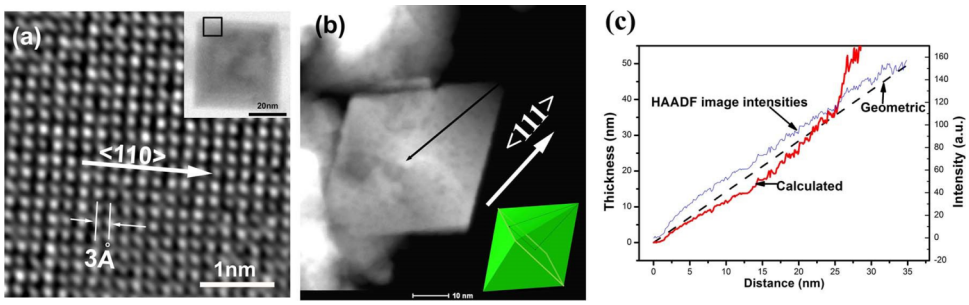

FIG. 4. (a) HRTEM image of the octahedron shown in the inset; view from <111>, the arrow indicates the <110> direction, (b) An HAADF image of an octahedron showing its shapes and a corresponding schematic below. (c) Intensity profiles of the HAADF image is plotted, and its geometrical thickness is plotted as the dashed line while the thickness calculated from image contrast is plotted as red bold line.

8-10 particles randomly selected) are defect free, which supports the single-crystalline nature of the Co_3O_4 octahedron.

It is well known that high angle annular dark field (HAADF) images show the mass thickness information of the materials, and the thickness of the sample can be deduced from its contrast by the following equation:[22]

$$t = -\frac{1}{\mu}\ln(1 - \frac{I}{I_0}) \tag{1}$$

where t is the thickness of the sample, μ is the attenuation coefficient, I is the measured intensity from the HAADF image and I_0 is the intensity of the incident beam. The thickness calculated from the HAADF image, as a function of location along the black line in Fig. 4(b), is shown as the red bold line in Fig. 4(c). The thickness value extracted from the contrast is consistent with that predicted from a solid regular octahedron (dashed lines in Fig. 4(c)). It indicates that our Co_3O_4 nanoparticles have a regular and solid octahedral geometry. The Co_3O_4 nanoparticles were formed through mild oxidation in the liquid phase. To reveal the formation mechanism, we have characterized the morphology of intermediate products at different reaction times. The evolvement of the microstructure and phase of these intermediate products (see the supplementary materials)[23] show that the $Co(OH)_2$ plates were first oxidized into CoOOH and then to Co_3O_4 within 60 min at 120 °C, which also confirms the XRD results (Fig. 1).

Figure 5(a) shows the magnetization data of the Co_3O_4 nano-octahedra as a function of temperature in an applied magnetic field of 1.0 T, carried out using two different samples. The nanoparticles show an antiferromagnetic phase transition at a Néel temperature T_N of 10 K, which is much less than the bulk value.[5] Furthermore the plot of the susceptibility in Fig. 5(b) shows that the paramagnetic Curie temperature θ is slightly positive, 3 ± 1 K, and the effective Bohr magneton number p_{eff} is 6.2 ± 0.3. The susceptibility is fitted to the equation

$$\chi = c + N_2 p_{eff}^2 \mu_B^2/(T-\theta), \tag{2}$$

where the number N_2 of Co^{2+} ions corresponds to one per formula unit. The expected spin-only value of p_{eff} for the bulk oxide is $g[S(S+1)]^{1/2}$ which is $\sqrt{15} = 3.9$ for high-spin Co^{2+}. However, there is usually a small orbital contribution to the Co^{2+} moment, so a typical experimental value of p_{eff} is about 4.8.[24] The observed susceptibility of our nanoparticles ($1.13 * 10^{-6}$ m^3 kg^{-1}) is twice as large as the bulk value (0.6×10^{-6} m^3 kg^{-1}).[25] The Co^{3+} ions at the B-sites normally have no moment, due to the large crystal-field splitting of the 3*d* orbitals by the octahedral cubic field. However, it has been shown both experimentally[24] and theoretically[13] that Co^{3+} may adopt a high-spin state on octahedral states near the surface. In some Co_3O_4 nanoparticles a shift of the field-cooled hysteresis loop has been attributed to exchange bias from a ferromagnetic surface layer on the particles.[7,26]

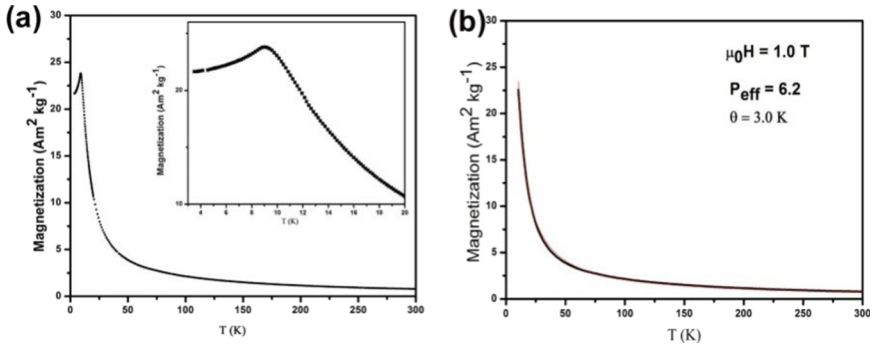

FIG. 5. Magnetic properties of Co_3O_4 nano octahedra (a) Temperature-dependence of magnetization for the Co_3O_4 nanooctahedra measured at $\mu_0H = 1.0$ T. The inset shows the enlargement of Fig. 5(a) in the low temperature region. (b) Plot of the susceptibility as a function of temperature. The susceptibility is fitted to the equation $\chi = c + N_2 p_{eff}^2 \mu_B^2/(T - \theta)$ (Equation (2)).

We can estimate the quantity of high-spin Co^{3+} in our nanoparticles derives from the excess susceptibility, the third term was added to equation (2) and susceptibility of our nanoparticles can be expressed in equation (3),[24]

$$\chi = c + N_2 p_{eff}^2 \mu_B^2/(T - \theta) + 2f N_3 p_{eff}^2 \mu_B^2/(T - \theta) \quad (3)$$

where f is the fraction of Co^{3+} in a high-spin state. Since the spin-only value of p_{eff} for high-spin Co^{3+}, S = 2 is $\sqrt{24} = 4.9$, and the usual experimental value is 5.4,[23] it follows that the fraction of high-spin Co^{3+} in our material is f = 0.36. This would correspond to a surface layer on a 30 nm particle that is 5 nm thick.

It is interesting to note that the presence of the high-spin Co^{3+} in the nanoparticles is associated with a shift towards a slight predominance of ferromagnetic interaction, as indicated by the reduction in the Néel temperature, and the slightly positive paramagnetic Curie temperature. Ferromagnetic exchange in mixed-valence spinel-structure oxides such as Fe_3O_4 is normally associated with electron hopping between B-sites occupied by high-spin ions of the same element in different charge states. Here we have the same ion in different spin states, and we speculate that the charge hopping might involve the following exchange

$$Co^{3+}(hs) + Co^{3+}(ls) \leftrightarrow Co^{4+}(hs) + Co^{2+}(hs) \quad (4)$$

In any case, most of the cobalt in the Co_3O_4 nanoparticles, unlike the bulk, is in a high-spin state.

IV. CONCLUSION

Octahedral Co_3O_4 nanoparticles 20-40 nm in size were synthesised in an aqueous ammonia solution using hexagonally shaped $Co(OH)_2$ nanoplates as starting materials. The octahedral Co_3O_4 nanoparticles have a spinel structure with <111> as their long axis and {111} facets exposed to the air. The Co_3O_4 nano-octahedra show an antiferromagnetic phase transition at a Néel temperature T_N of approximately at 10 K. Much of the Co^{3+} is in ahigh-spin state. In addition, the dimension of the nanoparticles can be controlled by varying the reaction parameters, e.g., the temperature and reaction time, which shows the controllability of the synthesis.

ACKNOWLEDGMENTS

The work at the School of Physics and the Centre for Research on Adaptive Nanostructures and Nanodevices at Trinity College Dublin is supported by Science Foundation Ireland under Grant 07/SK/I1220a. The TEM work was conducted under the framework of the INSPIRE program, funded by the Irish Government's Program for Research in Third Level Institutions, Cycle 4, National Development Plan 2007-2013.

[1] X.W. Lou, D. Deng, J.Y. Lee, and L. A. Archer, J. Mater. Chem. **18**, 4397 (2008).
[2] X. Wang, W. Tian, T. Zhai, C. Zhi, Y. Bando, and D. Golberg, J. Mater. Chem. **22**, 23310 (2012).
[3] W.Y. Li, L.N. Xu, and J. Chen, Adv. Fun. Mater. **15**, 851 (2005).
[4] X. Xie, Y. Li, Z.Q. Liu, M. Haruta, and W. Shen, Nature **458**, 746 (2009).
[5] W.L. Roth, J. Phys. Chem. Solids **25**, 1 (1964).
[6] X. Shen, H. Miao, H. Zhao, and Z. Xu, Appl. Phys. A: Mater. Sci. Process. **91**, 47 (2008).
[7] H.T. Zhu, J. Luo, J.K. Liang, G.H. Rao, J.B. Li, J.Y. Zhang, and Z.M. Du, Physica B: Condensed Matter **403**, 3141 (2008).
[8] M.J. Benitez, O. Petracic, H. Tüysüz, F. Schüth, and H. Zabel, Phys. Rev. B **83**, 134424 (2011).
[9] R.M. Wang, C.M. Liu, H.Z. Zhang, C.P. Chen, and L. Guo, Appl. Phys. Lett. **85**, 2080 (2004).
[10] T. Ambrose and C. L. Chien, Phys. Rev. Lett. **76**, 1743 (1996).
[11] R. Zhang and R. F. Willis, Phys. Rev. Lett. **86**, 2665 (2001).
[12] L. He, C. Chen, N. Wang, W. Zhou, and L. Guo, J. Appl. Phys. **102**, 103911 (2007).
[13] J. Chen and A. Selloni, Phys. Rev. B **85**, 085306 (2012).
[14] X. Wang, Y. Zhong, T. Zhai, Y. Guo, S. Chen, Y. Ma, J. Yao, Y. Bando, and D. Golberg, J. Mater. Chem. **21**, 17680 (2011).
[15] P. Lv, Y. Zhang, R. Xu, J.C. Nie, and L. He, J. Appl. Phys. **111**, 013910 (2012).
[16] X. Xiao, X. Liu, H. Zhao, D. Chen, F. Liu, J. Xiang, Z. Hu, and Y. Li, Adv. Mater. **24**, 5762 (2012).
[17] A. Fernández-Osorio, A. Vázquez-Olmos, R. Sato-Berru, and R. Escudero, Rev.Adv.Mater.Sci. **22**, 60 (2009).
[18] M.J. Kim and Y.D. Huh, Mater. Lett. **65**, 650 (2011).
[19] A. L. Patterson, Phys. Rev. **56**, 978 (1939).

[20] D. Zhou, M. Boese, R. Wang, and H. Zhang, J. Nanosci. Nanotechnol. **11**(12), 11028 (2011).
[21] Q. Chen, N. Wang, and L. Guo, Res. Chem. Intermed. **37**, 421 (2011).
[22] W. Van den Broek, A. Rosenauer, B. Goris, G.T. Martinez, S. Bals, S. Van Aert, and D. Van Dyck, Ultramicroscopy **116**, 8 (2012).
[23] See supplementary material at http://dx.doi.org/10.1063/1.4928494 for evolvement of the microstructure and phase of intermediate products.
[24] *Magnetism and Magnetic Materials*, edited by J. M. D. Coey (Cambridge University Press, London, 2010), p. 109.
[25] P. Dutta, M. S. Seehra, S. Thota, and J. Kumar, Journal of Physics: Condensed Matter **20**(1), 015218 (2008).
[26] E. L. Salabaş, A. Rumplecker, F. Kleitz, F. Radu, and F. Schüth, Nano Lett. **6**, 2977 (2006).